Currents through Torres Strait

ERIC WOLANSKI, PETER RIDD AND MASAMICHI INOUE*

Australian Institute of Marine Science, Townsville M.C., Queensland, Australia

(Manuscript received 16 November 1987, in final form 19 April 1988)

ABSTRACT

A five-month field study of the circulation in the Torres Strait was carried out. Baroclinic effects were negligible. The Arafura Sea and the Coral Sea forced a different tide on either side of Torres Strait, resulting in fluctuations of sea level difference of up to 6 m on either side of the Strait. The tidal dynamics in the Strait were controlled by a local balance between the acceleration, the sea level slope, and the bottom friction. Only 30% of the semidiurnal tidal wave was transmitted through Torres Strait. There were also fluctuations of the high-frequency sea level residuals (up to 0.8 m peak to trough) which appeared to be related to complex flows both through the Strait and across the Strait. Low-frequency sea level fluctuations were incoherent on either side of the Strait, and resulted in fluctuations of the low-frequency sea level differences on either side of the Strait of typically 0.3 m. These sea level gradients and the local wind forcing generated low-frequency current fluctuations through the Strait. These currents were small, being ≤ 0.1 m s^{-1}, because of the effect of friction which, at low-frequencies, was greatly enhanced by the nonlinear interaction between tidal and low-frequency currents. As a result, the Strait was also fairly impervious to long waves and there was only a negligible (for oceanic budget calculations) low-frequency transport through the Strait. The net current was only 0.01 m s^{-1} during the 5 months of observations, corresponding to a through-strait current of 10^{-2} sverdrups.

1. Introduction

The Torres Strait (hereafter referred to as the Strait) is the body of water connecting the Gulf of Carpentaria to the continental shelf of the Great Barrier Reef. The Strait thus theoretically enables an exchange of water between the Arafura Sea and the Coral Sea (Fig. 1). We call the Strait the rectangle whose long axis is oriented north–south and extends from Cape York Peninsula to Papua, New Guinea, and whose short axis is oriented east–west and is roughly 20 km wide extending from stations S5 to S8 (Fig. 1). The waters west of the Strait are shallow, shoaling westward, with depth of only 15 m, 40 km west of the Strait. East of the Strait, the shelf is fairly flat, the waters 15 to 20 m deep, with few reefs south of 10°S. The waters north of 10°S and west from 143°E (shown as stippled in Fig. 1) are not charted but are reported to be no more than 5 to 10 m deep with numerous shoals and reefs. The Strait itself is composed of several large coral reefs and coral-fringed islands. The reefs are elongated and typically 18 km long in an east–west direction, and separated by narrow channels, typically 1 to 3 km wide, 10 m deep, through which strong tidal currents have been reported. These reefs occupy 70% to 80% of the distance in a north–south direction. Long and narrow shoals, with water about 8 m deep, project into the Gulf of Carpentaria for another 20 km, and are located west of the islands and reefs of Torres Strait. The shapes of these shoals and reefs suggest that the currents are predominantly oriented east–west.

The water circulation in the Strait is poorly known. Even at present, the sea levels are fairly unpredictable and large ships rely on automatic real-time sea level observations, relayed by telemetry, to time their passage through the Strait. Wyrtki (1960) hypothesized that there was a strong seasonal current through the Strait bringing fresher water from the Gulf of Carpentaria and the Arafura Sea eastward into the Coral Sea in the (austral) summer and autumn. Wolanski and Ruddick (1981) and Wolanski et al. (1984a) have shown that this freshwater is more likely to originate from the Purari, Kikori and Fly Rivers discharging in the Gulf of Papua in the northwestern Coral Sea. Easton (1970) analyzed the then very sparse set of tidal data in the Strait and concluded that the cotidal lines were oriented approximately north–south, with strong gradients of phase and amplitude prevailing through the Strait. Amin (1978) studied the surges defined as tidal residual sea levels of period typically 2 to 5 days, and found that these were incoherent on either side of the Strait. In the absence of current data he was able to study neither the dynamics of these surges nor the tidal waves through the Strait. Wolanski and Ruddick (1981),

* Present affiliation: Coastal Studies Institute, Louisiana State University, Baton Rouge, Louisiana.

Corresponding author address: Dr. Eric Wolanski, Australian Institute of Marine Science, PMB No. 3, Townsville M.C., Queensland 4810 Australia.

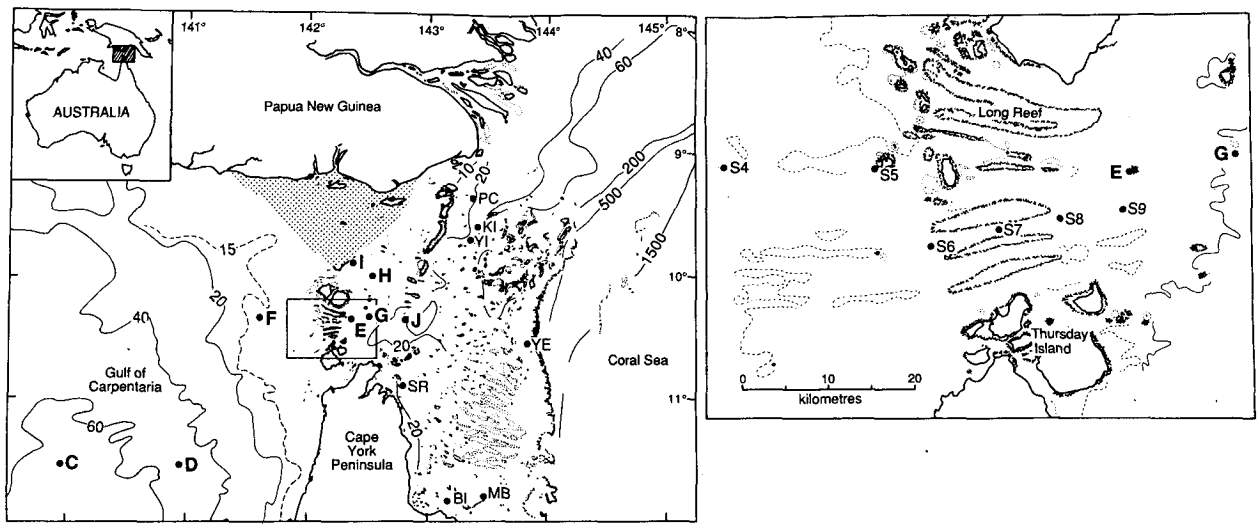

FIG. 1. Maps of the Torres Strait. Depths are approximate and given in meters. The shaded area represents an uncharted area believed to be between 5 and 10 m deep with numerous reefs and shoals. The circles and their corresponding labels correspond to moorings referred to in the text. In the small-scale chart, details of the 10 m isobath are shown.

Wolanski and Thomson (1984), Wolanski et al. (1984a) and Wolanski (1986) deployed current meters at sites on the northern Great Barrier Reef continental shelf (sites KI, YI, PC, YE, MB, BI and SR; Fig. 1) for periods of weeks to months. They found no evidence for strong sustained low-frequency (period >2.8 days) currents. Since strong low-frequency through-strait currents would presumably be reflected also in strong currents at some of the above sites, it was tentatively inferred that the net currents through Torres Strait were weak, much weaker than postulated by Wyrtki and Rochford (in Pickard et al. 1977). Using these data, Wolanski (1983) also showed that the tides over the continental shelf of the Great Barrier Reef are controlled by the tides of the Coral Sea, with no significant effect that could be attributed (at the measuring sites) to the tidal forcing by the Gulf of Carpentaria. The only current data in the Strait itself were from an Aanderaa current meter deployed for two months near Thursday Island (Fig. 1) in 1979. The data showed that the low-frequency through-strait currents were not only weak (always <0.1 m s^{-1}) but also reversed direction several times over the two month sampling period, so that the net flow through the Strait would have been minimal (Wolanski and Ruddick 1981). The data were too intermittent, for a detailed analysis of tidal and low-frequency currents, because of seaweeds frequently blocking the rotor of the current meter, though the rotor was cleared by divers at weekly intervals. This lack of information has forced various modellers of the circulation in the Gulf of Carpentaria (Church and Forbes 1981; Forbes and Church 1983; Rienecker 1979; Webb 1981) and on the continental shelf of the Great Barrier Reef (Wolanski and Thomson 1984) to make various unverified assumptions on the tidal and wind-driven currents through Torres Strait.

As part of the contribution of the Australian Institute of Marine Science to AMEX (the Australian Monsoon Experiment), we undertook a study of the physical oceanography of Torres Strait. The data enabled us to formulate and verify a model of the currents in the Strait. The data and the model are described below.

2. Methods

a. Oceanographic data

Aanderaa model WLR-5 water level recorders were bottom-mounted at sites (see Fig. 1) F (near Cook Reef), E (near Travers Islands), J (near Kirkcaldie Reef), and I (near Gariar Reef). These instruments recorded sea levels averaged over 56 seconds, at 30-minute intervals. Inter-Ocean model S4 current meters were deployed at 8 m above the bottom at sites G and H. These instruments recorded the currents averaged over 1 minute at 30 minute intervals. Sites G and H were several kilometers from the nearest reef or island, and so the currents were (presumably) not affected by the complex circulation near islands and through reef passages. All these instruments were deployed in October 1986 and recovered in March 1987. They yielded 100% data return, except for the current meter from site G which stopped working after three months due to battery failure. Three-hourly wind data at Thursday Island (TI) were also obtained from the Bureau of Meteorology. Additionally, we obtained from the Royal Australian Navy time series of hourly sea level data, spanning two months in 1985, at sites S4, S5, S6, S7, S8 and S9, on a transect through the Strait along Simpson Channel. Tidal harmonic constants were also obtained for the stations described by Amin (1978). Most of these stations are located west of Torres Strait.

Vertical profiles of temperature and salinity were obtained at a number of sites during cruises in October 1986, and March 1987.

b. *Data processing*

Tidal harmonic analysis (Foreman 1978) was used to calculate tidal constants for sea level and current data. These constants were then used to calculate time series of tidally-predicted sea levels and currents. Time series of the residuals were obtained by subtracting the tidally predicted time series from the observed ones. Time series of low-frequency residual sea level and currents were obtained by applying Godin (1972) moving average filter, $A_{24}^2 A_{25}/24^2 25$, to the time series of the residuals. Time series of high-frequency residual sea level and currents were obtained by subtracting the low-frequency residual data from the time series of residuals. The coherence computations followed the procedure of Raupach and Mitchell (1977). The oceanographic convention is used for the wind. Currents and wind velocity are positive if eastward (through the Strait) or northward (across the Strait). Thus a through-strait current is eastward, an across-strait current is northward. The time is expressed in day number in 1986/87, local time, 10 hours ahead of UTC.

3. Results

The spectrum of the sea level at site E (Fig. 2, line a) shows that the semidiurnal and diurnal tides contain the bulk of the tidal energy. There is a small amount of energy at the M_4 and MS_4 frequencies. More significantly, for periods >4 days, there is a significant variance increasing for longer periods. The tides are mixed semidiurnal on either side of the Strait (sites J and F, respectively lines a and b in Fig. 3), however they are incoherent through the Strait. For instance (see the lines X linking lines a and b in Fig. 3), spring tides at site F (Gulf of Carpentaria side of the Strait) can occur at neap tides at site J (Great Barrier Reef side of the Strait). This is due to a difference in the age of the tide as discussed by Easton (1970). As a result, the sea level difference through the Strait (line c, Fig. 3) is large, with tidal fluctuations reaching 6 m. The datum of the sea level is unknown and is assumed to be such that the mean sea level over the 5-month observation period was the same at all sites.

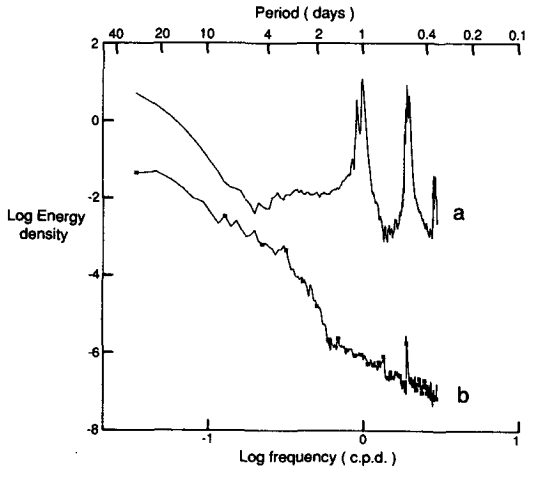

FIG. 2. Energy spectrum of the raw sea-level time series at site E (a), and (vertically displaced) of the residual sea-level time series at site E (b). The 90% confidence limits span about a decade of energy density.

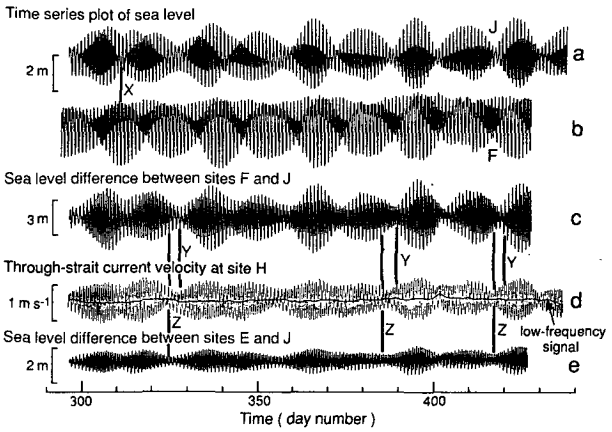

FIG. 3. Time series plots of the raw variables: the sea level at sites J (a) and F (b), the sea level difference between sites F and J (c), the through-strait current at site H (d), and the sea level difference between sites E and J (e). The thick line through line d represent the low-frequency signal. The datum of sea level is unknown and is assumed to be such that mean sea level over the 5-month observation period is the same at all sites. Time is expressed in day number in 1986/87, local time. The symbols X, Y and Z point to events in the spring–neap tide and are discussed in the text.

These sea level gradients generate strong tidal currents through the Strait. The tidal ellipses at sites G and H (Great Barrier Reef side of the Strait), for the four dominant constituents (O_1, K_1, M_2 and S_2), are shown in Fig. 4. The ellipses, particularly those at semidiurnal frequencies, have high eccentricities indicating that the tidal flow is mainly rectilinear and oriented approximately along the Strait. The phase lags

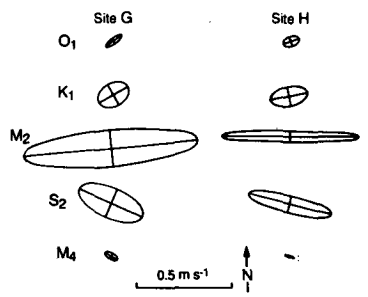

FIG. 4. Tidal ellipses at sites G and H for the four dominant constituents (O_1, K_1, M_2 and S_2), and for the M_4 constituent.

(not shown) between current meter sites G and H, between tide gauge sites I and E east of the Strait, and between tide gauge sites F and Booby Island (one of Amin's stations) west of the Strait, are small, indicating that these results are spatially coherent. The tidal currents are dominated by the semidiurnal constituents which give rise to peak semidiurnal tidal currents of several times those caused by the diurnal constituents.

We have also shown in Fig. 4 the tidal ellipse at sites G and H, at the M_4 frequency. Clearly, the strong semidiurnal currents do not produce strong overtides, contrary to the situation observed in other shallow waters such as estuaries and bays (Aubrey 1986).

Line d of Fig. 3 shows a time-series plot of the through-strait currents at site H (Great Barrier Reef side of the Strait). While these currents have a spring–neap tide cycle, it does not match the tide cycle of the sea level difference through the Strait (line c of Fig. 3). The lines "Y" indicate a 4-day phase shift between the spring–neap tidal cycles. However, the spring–neap cycle of the through-strait currents at sites G and H match somewhat more faithfully (see the lines marked "Z") that of the sea level difference between sites E and J (line e of Fig. 3), i.e. the local sea level slope east of the Strait. This observation suggests that the tides are not transmitted well through the Strait.

Our CTD data show no vertical structure in the density, the waters being everywhere well-mixed in temperature and salinity. Further, there were only minimal differences between the densities on either side of the Strait. Hence barotropic conditions prevailed. A time series plot of temperature at sites F and J is shown in Fig. 5. Clearly, the through-strait temperature gradients were negligible and too small to use the temperature as a tracer.

The low-frequency residual currents at sites G and H were predominantly through-strait, and typically less than 0.1 m s^{-1}, i.e., were only 10% to 20% of the tidal current amplitude (line d of Fig. 3). The through-strait low-frequency residual currents at sites G and H were coherent ($R^2 = 0.8$) one with the other (lines h and i, Fig. 6). They were marginally coherent with the through-strait wind velocity ($R^2 = 0.3$; line b of Fig. 6), but were highly coherent with the low-frequency residual sea level difference through the Strait ($R^2 = 0.8$; line g of Fig. 6). They were also highly coherent ($R^2 = 0.8$) with the difference (not shown) in low-frequency sea level between sites I and E, suggesting that, at low frequencies, the across-strait sea level slope

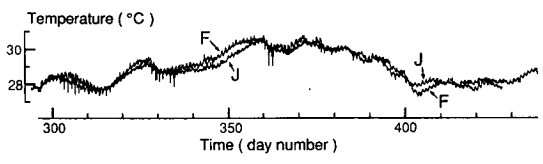

FIG. 5. Time series plot of the bottom temperature at the sites F and J.

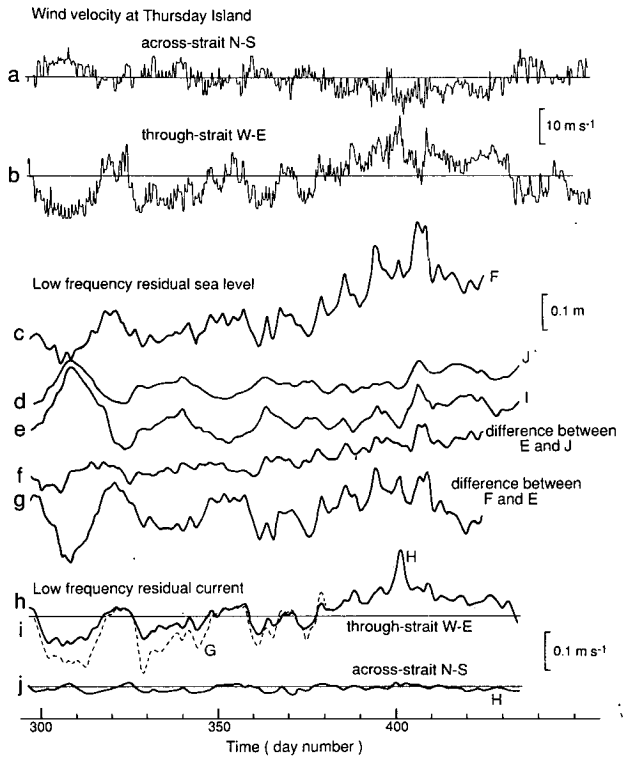

FIG. 6. Time series plot of the across-strait (a) and through-strait (b) wind velocity at Thursday Island, and of the low-frequency residual sea level at site F (c), J (d) and I (e), of the difference of the low-frequency residual sea level at sites E and J (f) and F and E (g), and of the low-frequency residual current at sites H (through-strait: i; across-strait: j) and G (through-strait: h).

was in geostrophic balance with the through-strait current. Both the across-strait wind velocity (line a of Fig. 6) and the across-strait low-frequency residual currents (line j of Fig. 6) were much smaller than, respectively, the through-strait wind velocity and water currents.

Time series plots of the low-frequency residual sea level fluctuations at sites F, J and I are shown in Fig. 6 (lines c, d and e respectively). The low-frequency residual sea level fluctuations were coherent ($R^2 \geq 0.5$) with each other for stations on one side of the Strait, but were incoherent ($R^2 \leq 0.2$) with each other for stations on either side of the Strait. This suggests that low-frequency sea level fluctuations in the Gulf of Carpentaria were not felt strongly east of the Strait. Note for instance from lines c, d and e, the apparent negative correlation between the sea level fluctuations on either side of the Strait between days 290 and 330. Note also that, between days 330 to 400, no correlation existed, and there were frequent fluctuations of sea level west of the Strait, which were not observed east of the Strait. The origin of these fluctuations has been attributed to wind-driven arrested topographic waves east of the Strait (Wolanski and Thomson 1984), and to both wind-driven fluctuations in the Gulf of Carpentaria and to events in the Arafura Sea west of Torres Strait

(Amin 1978). The origin of these fluctuations cannot be verified from our data because the spatial coverage was limited. These fluctuations were incoherent ($R^2 < 0.2$) with the through-strait wind. Low-frequency residual sea level fluctuations were typically 0.2 m peak to trough, an order of magnitude smaller than the fluctuations at tidal frequencies.

The difference in low-frequency residual sea level through the Strait (line g of Fig. 6) was marginally coherent ($R^2 = 0.3$), at zero phase lag, with the through-strait wind velocity (line b of Fig. 6), and was coherent ($R^2 = 0.5$) with the low-frequency sea level gradient east of the Strait (line f of Fig. 6).

The net current through the Torres Strait over the 5 months of observation was only about 0.01 m s^{-1}, i.e., too small to be reliably measured. This corresponds to a flux of only 10^{-2} Sv (Sv $\equiv 10^6$ m^3 s^{-1}), assuming that the Strait has a width of 10^5 m and a depth of 10 m.

The spectrum of the residual sea levels at site E (line b of Fig. 2) shows that the variance diminishes for decreasing periods, with a small peak near the semidiurnal frequencies. Hence nontidal energy is spread across the whole spectrum with no clearly preferred frequency.

The high-frequency residual sea level fluctuations east of the Strait (sites I and E in Fig. 7) were as large as 0.6 m peak to trough, but incoherent ($R^2 < 0.2$) between sites I and E, though some major features appear in both records. These fluctuations showed no clear spring–neap tidal cycle, contrary to observations in other shallow waters where such a cycle was observed (Provis and Lennon 1983).

Based on these observations, we propose below, and successfully test against the field data, one-dimensional models for the circulation at tidal and at low frequencies through the Strait. The model is not successful for the high-frequency residual motions probably because these are more two-dimensional.

4. Tidal wave transmission through Torres Strait

a. Tidal frequencies

We consider first the tidal frequencies. The Strait is schematized by a wave guide of uniform depth H_2,

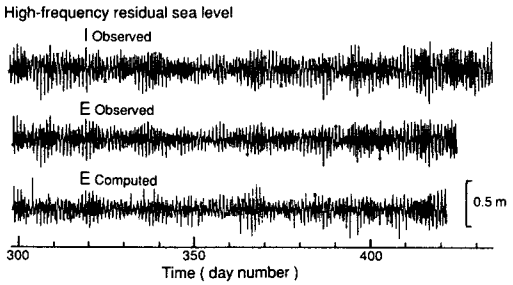

FIG. 7. Time series plot of the high-frequency residual sea level at site I (observed only) and E (observed and computed).

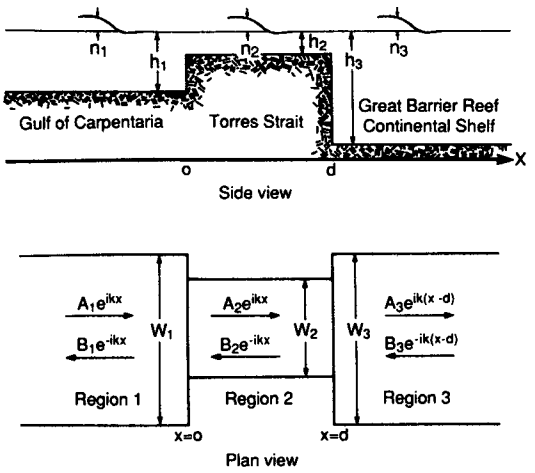

FIG. 8. Sketch of the waveguide model geometry.

linked to wave guides of uniform depth H_1 and H_3, and widths W_1 and W_3 respectively to the west and to the east of the Strait (Fig. 8). The Strait has a length d and a width W_2. The ratio W_2H_2/W_1H_1 is a measure of the degree of blockage of the through-strait currents by the reefs present in the Strait (Fig. 1). There are waves at tidal frequencies imposed on either side of the Strait. A fraction of these waves is reflected, another fraction is transmitted and the rest is dissipated by friction.

Assuming for the moment a linear bottom friction law, the linearized equations of motion, in each of the zones 1, 2 or 3 denoted by the subscript j ($j = 1$ to 3), are (Buchwald and Miles 1981)

$$\frac{\partial u_j}{\partial t} + g\frac{\partial \eta_j}{\partial x} + K_j\frac{u_j}{H_j} = 0 \tag{1}$$

$$H_j\frac{\partial u_j}{\partial x} + \frac{\partial \eta_j}{\partial t} = 0 \tag{2}$$

where x is distance, t time, g the acceleration due to gravity, η sea level and u velocity. Assuming that time dependence is of the form $\eta \propto e^{-i\omega t}$, where ω is the frequency, the solution to Eqs. (1) and (2) is, for regions $j = 1$ and 2

$$\eta_j = (A_je^{ik_jx} + B_je^{-ik_jx})e^{-i\omega t} \tag{3}$$

$$u_j = \frac{\sqrt{gH_j}}{H_jl_j}(A_je^{ik_jx} - B_je^{-ik_jx})e^{-i\omega t} \tag{4}$$

and for region $j = 3$,

$$\eta_3 = (A_3e^{ik_3(x-d)} + B_3e^{-ik_3(x-d)})e^{-i\omega t} \tag{5}$$

$$u_3 = \frac{\sqrt{gH_3}}{H_3l_3}(A_3e^{ik_3(x-d)} - B_3e^{-ik_3(x-d)})e^{-i\omega t} \tag{6}$$

where

$$k_j = \frac{\omega l_j}{\sqrt{gH_j}}, \quad l_j = (1 + i\epsilon_j)^{1/2},$$

$$\epsilon_j = \frac{K_j}{\omega H_j}, \quad i = (-1)^{1/2}. \quad (7)$$

The boundary conditions are

$$\eta_1 = \eta_2, \quad Fu_1 = u_2 \quad \text{at} \quad x = 0, \quad (8)$$

$$\eta_2 = \eta_3, \quad Fu_3 = u_2 \quad \text{at} \quad x = d, \quad (9)$$

where F^{-1} represents the fraction of the Strait not blocked by reefs and islands. The tidal harmonic constants are known from field observations at $x = 0$ and $x = d$. Because the equations are linear, Eqs. (1) to (9) are valid at each of the tidal frequencies. Hence, at each tidal frequency,

$$A_1 + B_1 = A_2 + B_2 = Z_1 \quad (10)$$

$$A_2 \exp(ik_2 d) + B_2 \exp(-ik_2 d) = A_3 + B_3 = Z_2 \quad (11)$$

$$A_1 - B_1 = \alpha(A_2 - B_2) \quad (12)$$

$$\beta[A_2 \exp(ik_2 d) - B_2 \exp(-ik_2 d)] = A_3 - B_3 \quad (13)$$

where Z_1 and Z_2 are the observed (through the tidal harmonic analysis) amplitudes and phases of the tides at $x = 0$ and $x = d$, the boundaries between the three regions. The boundaries were chosen to be $x = 0$ at 142°4′E (~3 km east of S5) and $x = d$ at 142°24′E (~4.5 km east of site E). The values of Z_1 and Z_2 were determined by linear interpolation along x, using the nearest tide gauge sites. In Eqs. (12) and (13):

$$\alpha = \frac{l_1\sqrt{H_1}}{Fl_2\sqrt{H_2}}, \quad \beta = \frac{l_3\sqrt{H_3}}{Fl_2\sqrt{H_2}}. \quad (14)$$

It is now simple algebra to solve the equations to obtain, for each tidal frequency, the values of the A_j and B_j (j = 1 to 3) as a function of Z_1 and Z_2, F, ω, K_j and H_j. The most suitable way to express the solution for numerical computations, is to find an expression for B_2 independently of the other coefficients A_j and B_j. It results

$$B_2 = \frac{Z_2 - Z_1 e^{ik_2 d}}{e^{-ik_2 d} - e^{ik_2 d}}. \quad (15)$$

Thereafter, we express the other coefficients A_j and B_j in terms of the coefficients which have already been evaluated. It results, in a sequential order for programming:

$$A_2 = Z_1 - B_2 \quad (16)$$

$$A_1 = 0.5[A_2(1 + \alpha) + B_2(1 - \alpha)] \quad (17)$$

$$B_1 = Z_1 - A_1 \quad (18)$$

$$A_3 = 0.5[A_2(1 + \beta)\exp(ik_2 d) + B_2(1 - \beta)\exp(-ik_2 d)] \quad (19)$$

$$B_3 = Z_2 - A_3. \quad (20)$$

To obtain maximum agreement between observed and predicted tidal data, the factor F was set equal to 3.5 (corresponding to the reefs and islands blocking 71% of the Strait), H_1, H_2 and H_3 were set equal to 11, 10 and 13 m respectively (a reasonable assumption), and (after about a hundred trial and error runs with the model), K_1, K_2 and K_3 were set equal to 2.5×10^{-3}, 6×10^{-3} and 2.8×10^{-3} m s^{-1} (also a reasonable assumption). The differences between K_i in the various regions are needed to obtain a good fit between observed and predicted tidal data, and can be seen as resulting from the fact that the more appropriate friction law is nonlinear. As a result, the apparent value of K in region 2 where the currents are the largest, should be larger than in regions 1 and 3 where the currents are much weaker.

We verified the model against the four dominant tidal frequencies, namely M_2, S_2, O_1 and K_1. The observed and predicted variations through Torres Strait of the amplitude and phase of the tide at these four frequencies are shown in Figs. 9 and 10. The agreement between the observed and theoretical results is very encouraging and suggests that the model, though very simple, has captured the essentials of the physics of the tidal propagation through Torres Strait. In view of this good fit, we have not judged it necessary to optimize the coefficients K_j by least square fits on the tidal constants for the four tidal constituents, because as is shown later, the linear friction law yields unrealistic results at low frequencies.

The primary advantage of this simple analytical model is that interpretation of the results is easy. $A_1 \exp(ik_1 x)$ and $B_3 \exp(-ik_3 x)$ represent the incoming waves from the Gulf of Carpentaria and the Coral Sea, respectively. It is possible to use this simple model to estimate the value of the reflection and transmission coefficients for a wave encountering region 2, which is the area of highest friction and blockage. Referring to Fig. 8, the propagation of a wave coming from the Gulf of Carpentaria can be modeled for $B_3 = 0$. The incoming wave (A_1) from the Gulf of Carpentaria propagates against an outgoing wave (B_1). A wave (A_2) propagates eastward in zone 2 (and decays by friction in the process since k is a complex number) against a westward moving reflected wave (B_2). A transmitted wave (A_3) propagates eastward in region 3. We chose to estimate the transmission coefficient of a wave going from the Gulf of Carpentaria to the Great Barrier Reef continental shelf. Because $H_1 \approx H_3$, the transmission coefficient is nearly identical for a wave going the other way. Using the model, it can be shown that the coefficients of reflection (R) and transmission (T) are

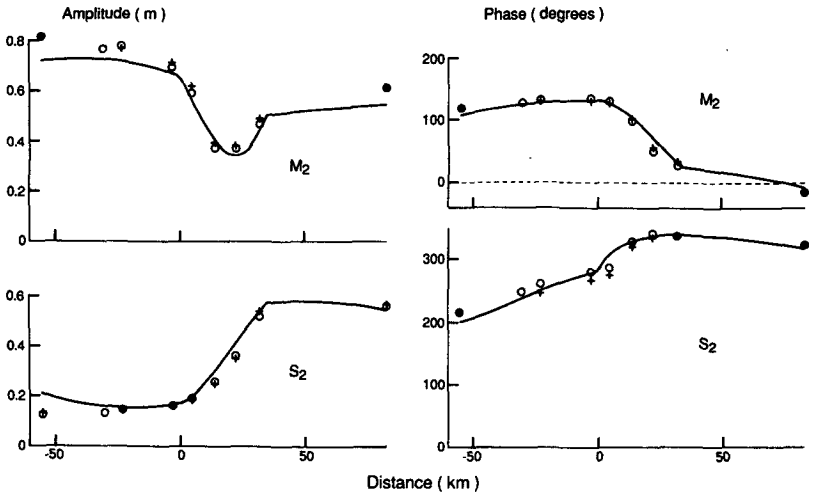

FIG. 9. Variation through the Strait of the amplitude and phase of the tide at the M_2 and S_2 frequencies, observed (circles), predicted by the linear analytical model (line), and predicted by the non-linear numerical model (crosses). Local phases are used. To convert to UTC, subtract 290° and 300° for respectively the M_2 and S_2 constituents.

$$R = B_1/A_1$$

$$= \frac{(1-\alpha)\left(1+\frac{1}{\beta}\right)e^{-ik_2d} + (1+\alpha)\left(1-\frac{1}{\beta}\right)e^{ik_2d}}{(1+\alpha)\left(1+\frac{1}{\beta}\right)e^{-ik_2d} + (1-\alpha)\left(1-\frac{1}{\beta}\right)e^{ik_2d}} \quad (21)$$

$$T = A_3/A_1$$

$$= \frac{4}{(1+\alpha)\left(1+\frac{1}{\beta}\right)e^{-ik_2d} + (1-\alpha)\left(1-\frac{1}{\beta}\right)e^{ik_2d}}. \quad (22)$$

For semidiurnal tides, $R = 0.68 \exp(i\,6°)$ and $T = 0.29 \times \exp(i\,45°)$.

For diurnal tides, $R = 0.63 \exp(-i\,11°)$ and $T = 0.36 \exp(i\,36°)$.

It is interesting to note that the transmission coefficient increases with increasing period. At semidiurnal frequencies, $|T| = 0.29$, while at diurnal frequencies $|T| = 0.36$.

This finding suggests that the transmission coefficient increases with increasing period. Indeed, the model suggests that at periods of 2, 4, 8 and 16 days, $|T|$ is 0.45, 0.54, 0.63 and 0.71, respectively. This prediction disagrees with the observations described above, that the low-frequency residual sea level fluctuations essentially do not propagate through the Strait. This discrepancy is removed below by including nonlinear effects in the model.

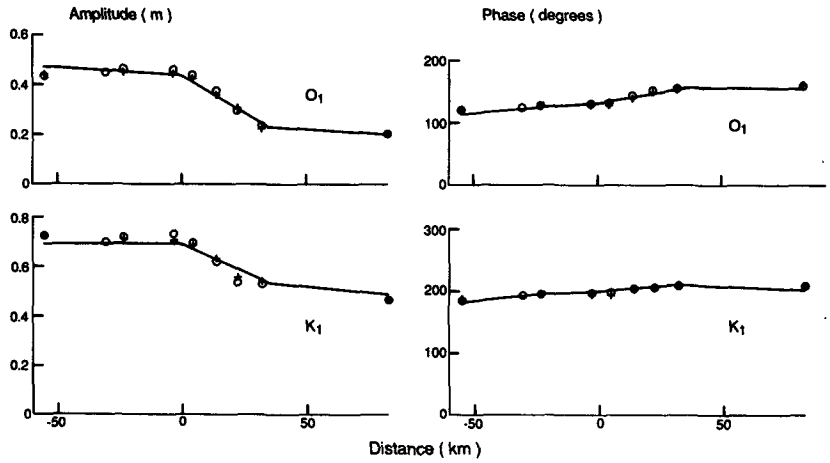

FIG. 10. As in Fig. 9 for the O_1 and K_1 frequencies. Local phases are used. To convert to UTC, subtract 139° and 150° for the O_1 and K_1 constituents, respectively.

5. Low-frequency currents through Torres Strait

It is often the practice to model the tidal and low-frequency (wind-driven) circulations independently. There are at least two difficulties with this approach in Torres Strait. First, the tidally-averaged depth-averaged momentum equation is nonlinear. In this equation, the tidal stress term

$$\frac{\partial}{\partial x}(\overline{u'^2}),$$

where u' is the tidal velocity and the overbar indicates a tidal average, can be expected to make a significant contribution in the presence of spatially varying strong tidal currents, as has already been demonstrated may indeed be the case on the shelf east of Torres Strait (Wolanski and Thomson 1984). Second, the bottom friction term in that equation varies with the square of the total velocity (tidal + low-frequency + high-frequency), and it is thus unrealistic to expect to calculate separately the friction due to tidal, low-frequency and high-frequency currents. In some cases, it may be possible to parameterize the bottom friction coefficient for low-frequency currents as a function of the maximum tidal current (Winant and Breadsley 1979; Csanady 1982), but this approach would be empirical and, further, would neglect the spring–neap tidal cycle.

In what follows, we return to the waveguide model used earlier, but we now include the nonlinear terms in the equations of motion, including a quadratic bottom friction law. We assume a one-dimensional channel, similar to that sketched in Fig. 8 (bottom), extending from site F to site J, and forced at site F and J by the observed sea levels. These observed sea levels contain, among other things, the tides, the high-frequency tidal residuals and the low-frequency residual sea level fluctuations that may arise from large-scale dynamics on the Gulf of Carpentaria and the Great Barrier Reef continental shelf. The equations of motion for one-dimensional open-channel flow are (Harleman 1971),

$$\frac{\partial A}{\partial t} + \frac{\partial Q}{\partial x} = 0 \tag{23}$$

$$\frac{\partial Q}{\partial t} + \frac{\partial}{\partial x}(Q^2/A) + gA\frac{\partial}{\partial x}(y+z) + gAS_f - \tau W = 0 \tag{24}$$

where x is the distance from site F through the Strait, t is the time, Q the discharge, A the cross-sectional area, g the acceleration due to gravity, z the elevation of the bottom above datum, y the total depth $(H+\eta)$, τ the wind stress and S_f is the frictional slope where, in metric units,

$$S_f = \frac{n^2 Q|Q| B^{4/3}}{A^{10/13}} \tag{25}$$

where n is the Manning roughness coefficient and B the wetted perimeter. The wind stress was computed from the wind data at Thursday Island. Our channel has a width $W_1 = W_3 = 800$ m, $W_2 = 250$ m. The actual values of W_i are irrelevant provided $W_i \gg H_i$ and that the ratio W_1/W_2 represents the appropriate blocking of the flow in region 2 by reefs and islands. The channel comprised 24 sections, 3 of them being in the Strait. The bottom is not flat and the values of $z(x)$ at each cross section were taken from bathymetric charts. The equations (28) to (30) were solved numerically using the iterative fully implicit finite difference scheme described by Wolanski et al. (1980).

The advantage of the numerical model over the analytical model is that it is more realistic. Indeed, in the latter, the friction law is linear and the friction coefficient (K_i) has to vary empirically from region to region, while in the former, the friction law is nonlinear and the friction coefficient (n) is kept uniform (0.025) in space and time because it parameterizes only bottom roughness. Further, tidal and nontidal effects are included simultaneously so that the friction is represented more accurately.

The model yields encouraging results at tidal frequencies. The variation through the Strait of the amplitude and phase of the tide at the dominant diurnal and semidiurnal frequencies is shown in Figs. 9 and 10. The comparison between observed and predicted variations is encouraging. The numerical model predicts these dominant tidal constituents at least as well as the analytical model. A visual comparison between observed and computed tidal currents at site G, is encouraging (see Fig. 11), though there are some discrepancies, for instance from days 340 to 355 and from days 365 to 385.

The model was also used to estimate the likely influence that the islands and reefs have on the water circulation at tidal frequencies. This was done by running the model with the same boundary conditions but with different values of the ratio W_1/W_2. The observed and predicted values of the tidal currents at site G were then compared. The observed peak to trough current fluctuations for the spring tides around day no. 370, were 1.05 m s^{-1}. The computed ones were 0.44, 0.94, 1.21, 1.61 and 2.12 m s^{-1} for the ratio W_1/W_2 set equal to, respectively, 8, 4, 2, 1.67 and 1.15. Fur-

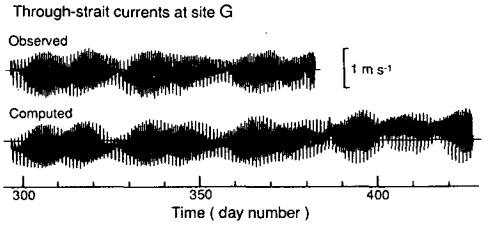

FIG. 11. Time series plot of the observed and computed through-strait currents at site G.

ther, the phase of the tidal constituents at site G was also modified by these changes, because the timing of the spring–neap tidal cycle was shifted by several days (up to 6, not shown) with the above changes in W_1/W_2. Note that, by continuity, the tidal currents are expected to be about five times larger in the passages than at site G which is located east of the passages.

These findings suggest that the islands and reefs, by constricting the flow through the Strait to a few passages, largely control the tidal propagation through the Strait. A more accurate determination of the influence of islands and reefs would require a two-dimensional model.

The model also yields encouraging results at low frequencies. Figure 12 shows the close agreement ($R^2 = 0.8$) between observed and numerically predicted low-frequency residual sea levels at site E. There is also an encouraging agreement ($R^2 = 0.7$) between observed (line a, Fig. 13) and numerically predicted (line d, Fig. 13) low-frequency residual through-strait currents at site G. The model thus explains 70% of the low-frequency current variability. Line b of Fig. 13 shows the numerically predicted currents in the absence of tides and of low-frequency sea level gradients. Line c shows the numerically predicted currents in the absence of tides but including the observed low-frequency residual sea levels at sites F and J. In all cases the Manning coefficient was kept constant ($n = 0.025$). The comparison between lines b and c shows the importance of the externally imposed sea level gradient through the Strait. The comparison between lines c and d shows the importance of the tidal currents in increasing the apparent value of the bulk friction coefficient for low-frequency currents. As a result, the low-frequency currents through the Strait are typically only ⅓ to ¼ their expected values in the absence of tides.

The model also yields high-frequency residual motions and these are discussed below.

6. High-frequency residual motions

A time series plot of the numerically predicted high-frequency residual sea level at site E is shown in Fig. 7 and this should be compared with the observed one also shown. The coefficient of correlation (at zero time lag) between these observed and computed time series is only about 0.55. This implies that a significant fraction of the high-frequency residual fluctuations cannot be accounted for by the one-dimensional propagation, towards the Strait, of events (waves) traveling past sites F and J. This suggests that the high-frequency residual motions may be two-dimensional. Presumably, they could take the form of waves propagating northward or southward and trapped by the Strait forming a (porous) waveguide. The simplest equation of motion for such waves would be

$$\frac{\partial v''}{\partial t} = -g\frac{\partial \eta''}{\partial y} \tag{26}$$

where v'' is the high-frequency residual current along the y axis oriented northward, and η'' is the high-frequency residual sea level. Coriolis effects may also be present, and in these shallow waters friction would rapidly, in less than a day, destroy such waves if they were free. Equation (26) would imply a 90° phase lag between v'' and $\partial\eta''/\partial y$. In fact, there is evidence for this in the observed coherence and phase relationship, shown in Fig. 14, between, on the one hand, the difference between the high-frequency residual sea levels at sites I and E, and, on the other hand, the high-frequency residual northward current at site H. There are several intervals in the period domain where there is a high coherence between these variables, and in such intervals there is about a 90° phase lag. The origin of these waves is still unclear.

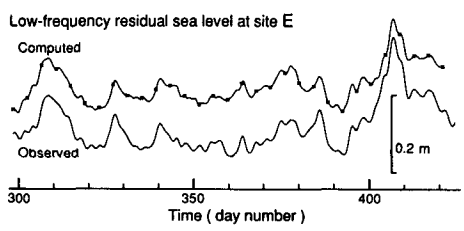

FIG. 12. Time series plot of the observed and computed low-frequency residual sea level at site E.

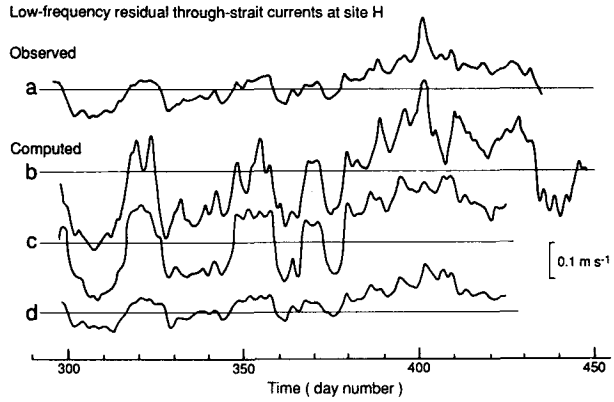

FIG. 13. Time series plot of the low-frequency residual through-strait currents, observed at site H (a) and computed under various hypotheses (b to d) described in the text.

7. Conclusion

Because the tides are incoherent on either side of the Strait, large sea level differences are experienced through the Strait. These differences drive strong tidal currents, which are magnified by the flow channelization in the passages through the Strait. The tidal wave dynamics in the Strait result from a balance between acceleration, sea level slope and bottom friction. A one-dimensional model appears to be successful in capturing these essential physics. Only about 30% of a tidal

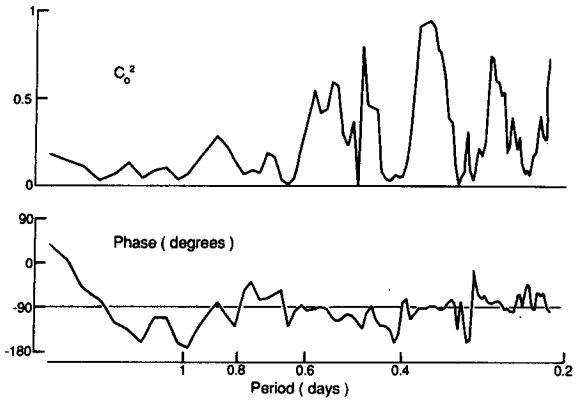

FIG. 14. Variation with period of the coherence squared (C_0^2) and the phase (θ) between, on the one hand, the difference of the high-frequency residual sea level at sites I and E, and, on the other hand, the high-frequency residual across-strait current at site H. The 90% confidence level of C_0^2 is about 0.3.

wave approaching Torres Strait from east or west is transmitted through the Strait.

The low-frequency sea levels are incoherent on either side of the Strait, and result in large low-frequency sea level slopes through the Strait. This slope, together with the local wind stress, may be expected to drive strong low-frequency currents at least in Torres Strait. However, this was not observed and the discrepancy is explained by the nonlinearity of the equations of motion. It is shown that the tidal stress increases by nearly an order of magnitude the value of the bulk friction coefficient for low-frequency currents from its estimated value based on low-frequency currents alone. This demonstrates that tidal and low-frequency currents cannot be modeled independently.

The models are successful in reproducing a number of observations of tidal and low-frequency motions. They are, however, one-dimensional and need to be extended to cover two-dimensional motions. For practical applications, or for more detailed studies, two-dimensional models may need also to include the details of the flows around reefs and islands and through the passages in the Strait where island wakes and tidal jets are present and have been observed (Wolanski et al. 1984a). Such motions can be incorporated in two-dimensional models (Falconer et al. 1986; Wolanski et al. 1984b, 1988).

The barotropic through-strait current U must be smaller than the maximum value determined by hydraulic control, so that $U < (gH)^{1/2} \approx 10$ m s^{-1}. Nof (1988) showed that the vorticity control can reduce the flux to a few percent of that associated with the hydraulic control. When, as can be expected to happen at unsteady state, the intrusive water mass occupies only a fraction of the width $W \approx 10^5$ m (i.e., of the distance between Australia and Papua New Guinea) of the Strait, he proposed that $U < fW/10 \approx 0.5$ m s^{-1}. Our observations show that the low-frequency current $U \leq 0.1$ m s^{-1}, which is even smaller than the limit set by the vorticity control. This suggests that another process limits even further the flux through Torres Strait, and our model suggests it is bottom friction.

The high-frequency residual sea level fluctuations, responsible for much of the unexplained variance, appear to be due to waves propagating both through and across the Strait. The origin of these waves is still unclear.

The Torres Strait may be the only Strait so far studied where baroclinic motions are negligible.

The current meter data show a seasonality of the currents, with currents from the Arafura Sea to the Coral Sea during the northwesterly monsoon season, and from the Coral Sea to the Arafura Sea during the southeast trade wind season. However, these currents were weak and, because of the small depths of water, the exchange of water through the Torres Strait between the Arafura Sea and the Coral Sea, was negligible for oceanic budget calculations.

Acknowledgments. It is a pleasure to acknowledge the field assistance of Mr. R. McAllister, Mr. J. Sodusta, Mr. C. Villanoy, Mr. S. Power and Mr. N. Harcock (who all survived the "enjoyable" AMEX cruises), the skippers of the research vessel R.V. *Lady Basten,* Mr. J. Futcher and Mr. D. Beard, and Ms. M. Thyssen who drew the figures. Two reviewers criticized and improved the manuscript.

REFERENCES

Amin, M., 1978: A statistical analysis of storm surges in Torres Strait. *Aust. J. Mar. Freshwater Res.*, **29,** 479–496.

Aubrey, D. G., 1986: Hydrodynamics controls on sediment transport in well-mixed bays and estuaries. *Physics of Shallow Estuaries and Bays,* J. Van de Kreeke, Ed., 245–258, Springer-Verlag.

Buchwald, V. T., and J. W. Miles, 1981: On resonance of off-shore channels bounded by a reef. *Aust. J. Mar. Freshwater Res.*, **32,** 833–841.

Church, J. A., and A. M. G. Forbes, 1981: A non-linear model of the tides in the Gulf of Carpentaria. *Aust. J. Mar. Freshwater Res.*, **32,** 685–697.

Csanady, G. T., 1982: *Circulation in the Coastal Ocean.* Reidel, 279 pp.

Easton, A. K., 1970: The tides on the continent of Australia. Horace Lamb Center for Oceanographic Research, Adelaide, Res. Paper No. 37.

Falconer, R. A., E. Wolanski and L. Mardapitta-Hadjipandeli, 1986: Modeling tidal circulation in an island's wake. *J. Waterway, Port, Coastal Ocean Eng.*, **112,** 234–254.

Forbes, A. M. G., and J. A. Church, 1983: Circulation of the Gulf of Carpentaria. II: Residual currents and mean sea level. *Aust. J. Mar. Freshwater Res.*, **34,** 11–22.

Foreman, M. G. G., 1977: Manual for tidal height analysis and prediction. Pacific Marine Science Rep. 77–10, 97 pp., Institute of Ocean Science, Patricia Bay, Sidney, British Columbia.

Godin, G., 1972: *The Analysis of Tides.* Toronto University Press.

Harleman, D. R. F., 1971: One-dimensional models. *Estuarine Modelling, An Assessment.* Water Quality Office, U.S. Environmental Protection Agency, 16070 DZV 02/71, Washington D.C.

Nof, D., 1988: Vorticity control. *J. Phys. Oceanogr.*, in press.

Pickard, G. L., J. R. Donguy, and F. Rougerie, 1977: A review of the physical oceanography of the Great Barrier Reef and western

Coral Sea. Australian Institute of Marine Science, Monogr. Ser. No. 2, pp. 134.

Provis, D. G., and G. W. Lennon, 1983: Eddy viscosity and tidal cycles in a shallow sea. *Estuarine, Coastal Shelf Sci.*, **16,** 351–361.

Raupach, M., and W. Mitchell, 1977: Time series analysis on the Dec-System-10. Computing Report No. 10. Flinders Institute for Atmospheric and Marine Science, Flinders University.

Rienecker, M. M., 1979: Tidal propagation in the Gulf of Carpentaria. Ph.D. thesis, University of Adelaide.

Webb, D. J., 1981: A numerical model of the tides in the Gulf of Carpentaria and the Arafura Sea. *Aust. J. Mar. Freshwater Res.*, **32,** 31–44.

Winant, C. D., and R. C. Breadsley, 1979: A comparison of shallow currents induced by wind stress. *J. Phys. Oceanogr.*, **9,** 218–220.

Wolanski, E., 1983: Tides on the northern Great Barrier Reef continental shelf. *J. Geophys. Res.*, **88,** 5953–5959.

——, 1986: The physical oceanography of Torres Strait. A. K. Haines, G. C. Williams and D. Coates, Eds., Torres Strait Fisheries Seminar, 275–291, Australian Govt. Publ. Service, Canberra.

——, M. Jones and J. S. Bunt, 1980: Hydrodynamics of a tidal creek–mangrove swamp system. *Aust. J. Mar. Freshwater Res.*, **31,** 431–450.

——, and B. Ruddick, 1981: Water circulation and shelf waves in the northern Great Barrier Reef lagoon. *Aust. J. Mar. Freshwater Res.*, **32,** 721–740.

——, and R. E. Thomson, 1984: Wind-driven circulation on the northern Great Barrier Reef continental shelf in summer. *Estuarine, Coastal Shelf Sci.*, **18,** 271–289.

——, G. L. Pickard and D. L. B. Jupp, 1984a: River plumes, coral reefs and mixing in the Gulf of Papua and the northern Great Barrier Reef. *Estuarine, Coastal Shelf Sci.*, **18,** 291–314.

——, J. Imberger and M. L. Heron, 1984b: Island wakes in shallow coastal waters. *J. Geophys. Res.*, **89,** 10 553–10 569.

——, E. Drew, K. Abel and J. O'Brien, 1988: Tidal jets, nutrient upwelling, and their influence on the productivity of the alga *Halimeda* in the Ribbon Reefs, Great Barrier Reef. *Estuarine, Coastal Shelf Sci.*, **26,** 169–201.

Wyrtki, K., 1960: Surface circulation in the Coral and Tasman Seas. CSIRO Division of Fisheries and Oceanography, Tech. Paper No. 8.